Biochemical and Biophysical Research Communications 450 (2014) 25–29

Contents lists available at ScienceDirect

Biochemical and Biophysical Research Communications

journal homepage: www.elsevier.com/locate/ybbrc

The Fe-heme structure of met-indoleamine 2,3-dioxygenase-2 determined by X-ray absorption fine structure

Jade B. Aitken [a,b,c], Christopher J.D. Austin [a,d], Nicholas H. Hunt [d], Helen J. Ball [d], Peter A. Lay [a,*]

[a] School of Chemistry, The University of Sydney, NSW 2006, Australia
[b] Australian Synchrotron, Clayton, Victoria 3168, Australia
[c] Institute of Materials Structure Science, KEK, Tsukuba, Ibaraki 305-0801, Japan
[d] Department of Pathology and Bosch Institute, The University of Sydney, Camperdown, NSW 2006, Australia

ARTICLE INFO

Article history:
Received 7 May 2014
Available online 22 May 2014

Keywords:
Indoleamine 2,3-dioxygenase-2 (IDO2)
X-ray absorption fine structure
EXAFS
Heme environment
Mixed-spin species

ABSTRACT

Multiple-scattering (MS) analysis of EXAFS data on met-indoleamine 2,3-dioxygenase-2 (IDO2) and analysis of XANES have provided the first direct structural information about the axial donor ligands of the iron center for this recently discovered protein. At 10 K, it exists in a low-spin bis(His) form with Fe–N_p(av) = 1.97 Å, the Fe–N_{Im} bond lengths of 2.11 Å and 2.05 Å, which is in equilibrium with a high-spin form at room temperature. The bond distances in the low-spin form are consistent with other low-spin hemeproteins, as is the XANES spectrum, which is closer to that of the low-spin met-Lb than that of the high-spin met-Mb. The potential physiological role of this spin equilibrium is discussed.

1. Introduction

L-Tryptophan (Trp) is the least abundant, essential amino-acid in mammals [1]. The major route for human Trp metabolism (~90% of all ingested Trp) is the 'Kynurenine Pathway' (KP), which leads to the production of biologically active kynurenine metabolites [2], nicotinamide adenine dinucleotide and niacin [3,4]. The first, rate-limiting step of the KP is the oxidative cleavage of the 2,3-double bond of the indole ring of Trp to form *N*-formylkynurenine. Since the 1960s, this reaction was believed to be catalyzed by two heme-containing dioxygenases, the constitutively expressed tryptophan 2,3-dioxygenase (TDO) [5] and the inflammatory cytokine-induced indoleamine 2,3-dioxygenase-1 (IDO1) [6]. More recently it has been found that mammals possess a third dioxygenase enzyme capable of catalysing the oxidative cleavage of Trp, subsequently named indoleamine 2,3-dioxygenase-2 (IDO2) [7–9]. The discovery of a third initiating protein of the KP has attracted considerable research interest due to the established roles of Trp metabolism [10] and TDO/IDO1 dysfunction in numerous pathological conditions, including cancer [11,12] and malaria [13,14].

Phylogenetic analysis suggests that IDO1 arose in mammals from the gene duplication of an ancestral IDO2-like gene approximately 300 million years ago [15]. Interestingly, while modern IDO1 and IDO2 proteins share some amino acid sequence identity (43% for both the human and mouse proteins) [16], both enzymes show little similarity to TDO, indicating functional convergence in Trp metabolism evolution [9]. This evolutionary diversity is reflected in the distinct tissue expression patterns of each enzyme. In mammals, TDO is primarily expressed in the liver [17]. IDO1, in contrast, is found in almost all tissues and non-hepatic organs [18], including the intestine, placenta, lung, endocrine glands and central nervous systems [19–21]. IDO2 is primarily expressed in the kidney, reproductive tract, and liver [7].

IDO1 is a monomeric protein (MW 42 kDa) that is inactive in its native ferric form. IDO1 metabolic activity requires a reductant co-factor in order to bind Trp with high affinity [22]. *In vitro* IDO1 assays generally use a methylene blue/ascorbic acid reduction system, but the physiological reductant is suggested to be cytochrome b_5 [23]. Similarly IDO2 (MW 42 kDa) must be reduced to its ferrous form for enzymatic activity and cytochrome b_5 is the most efficient reductant *in vitro* [16].

Multiple-scattering (MS) analyses of EXAFS have been used for the structural characterizations of met- and deoxy-myoglobin (Mb) [24], as well as the NO adducts of IDO1 [25]. The validity of the EXAFS model used here has been verified for deoxy- and met-Mb by comparison of the EXAFS-derived bond lengths with those found in subsequent very high resolution XRD structures (~1 Å) [26,27]. The crystal structure of human IDO1 [28] has been used previously to model a likely structure for IDO2 (mouse) [16];

* Corresponding author.
E-mail address: peter.lay@sydney.edu.au (P.A. Lay).

http://dx.doi.org/10.1016/j.bbrc.2014.05.054
0006-291X/

however, the fine details of the active site/heme structure have not yet been determined experimentally. Hence, we report the first structural information on the heme moiety of mammalian IDO2 protein (*i.e.*, mouse met-IDO2) as determined by multiple-scattering analyses of extended X-ray absorption fine structure (EXAFS).

2. Materials and methods

2.1. Protein preparation

Cloning of the mouse IDO2 cDNA into the pDEST-17 for bacterial-expression of N-terminal 6× His tagged proteins has been described previously [16]. Briefly, cultures of transformed KRX *Escherichia coli* cells (Promega) were grown at 37 °C in 1 L of Terrific Broth medium supplemented with carbenicillin (50 mg/mL) until an OD_{600nm} of 0.8 was reached. The temperature was lowered to 20–22 °C until the OD_{600nm} was between 1.0 and 1.5. Then, expression of a heme-containing IDO2 protein was induced overnight by adding *iso*-propyl βD-1-thiogalactopyranoside (1 mM), rhamnose (0.1% w/v) and the heme precursor, δ-aminolevulinic acid hydrochloride (0.5 mM). KRX *E. coli* were collected by centrifugation at 8000*g* for 15 min, resuspended and incubated for 1 h on ice in 25 mM Tris buffer pH 7.4, 150 mM NaCl, 10 mM imidazole, 10 mM $MgCl_2$, lysozyme (1 mg/mL), EDTA-free cocktail inhibitor tablets (2×), DNase (<1 mg) and 1 mM phenylmethylsulfonyl fluoride (PMSF). The suspension was sonicated (Branson Sonifier 3 × 40 W, 30 s pulses) before clearing the supernate by centrifugation at 5000*g* for 20 min.

The supernate (25 mL) obtained from 1 L of culture was applied to a 1 mL Hi-Trap chelating column (Amersham Biosciences) that had been charged with nickel ions and equilibrated with basal buffer (25 mM Tris–HCl pH 7.4, 150 mM NaCl, 1 mM PMSF, 10 mM imidazole). After washing with 18 mL of basal buffer, the protein was eluted by gradually increasing the concentration of imidazole from 10 mM to 300 mM. Fractions with a high A_{406}:A_{280} ratios (*i.e.*, Soret heme absorbance to protein absorbance ratio) were pooled, desalted into 50 mM Tris–HCl pH = 7.4, 40% glycerol and concentrated to 1 mM using an Amicon Ultra 4 mL centrifugal device (Millipore) with a cut-off of 30000 kDa (utilising IDO2 protein preparations from a total of 28 L of bacterial culture). The protein was stored at −80 °C before analysis.

2.2. X-ray absorption spectra (XAS) data collection

The iron K-edge XAS of the met-IDO2 was recorded at SSRL on beamline 7–3 with a harmonic rejection mirror fully tuned. Data were collected as fluorescence spectra, using a Canberra 30-element Ge detector. The samples were held at a temperature of 10 K using an Oxford Instruments continuous-flow liquid helium cryostat. A calibration channel with an Fe foil was used to account for energy shifts in the monochromator [29]. The energy of the incident beam was calibrated with an iron foil, setting the first inflection point to 7111.2 eV, throughout an E_0 of 7130.0 eV was used. During the collection of data, the edge of each XAS spectrum was monitored for photodecomposition; due to photodamage only one scan was collected on each spot (12 scans in total, with two samples).

2.3. XAFS model

The porphyrin fragment was modelled in two-dimensional space [30] and with fourfold symmetry (Fig. S1). A number of models were considered for both adducts with the S_0^2 value set at 0.97, as was determined for met-myoglobin [24]. The models were: (i) a five-coordinate heme protein with the imidazole ring of the histidine as the proximal axial ligand, as described previously [24,25,30]; (ii) with an aqua ligand as the distal ligand; (iii) one with two *N*-bound histidines; and (iv) another with one *N*-bound and one *C*-bound histidines. The *C*-bound model was included as isomerisation between *N*- and *C*-bound imidazoles in complexes of Ru(II) and Ru(III) has previously been reported [31]; it is conceivable that such isomerisation could also be present in low-spin Fe(III) complexes. A complete set of restraints and constraints for these models is contained in the Supporting Information (Table S1) where σ_{res} is analogous to the estimated standard deviation.

MS analyses of XAFS data were performed using the XFIT program, which employed non-linear least-squares fitting of the XAFS spectrum, through the minimization of the sum of the square of the residuals [24,32]. XFIT integrates the FEFF6.01 program in its model fitting calculations, which included multiple-scattering codes [33,34]. The goodness-of-fit parameter (R) and Monte Carlo calculations were performed as reported previously [24,30,35,36]. The rms (root mean square) errors that result from the Monte Carlo analysis were combined with systematic errors to obtain the final conservative error estimate [30]. All background subtraction, splining, and normalization procedures were performed using XFIT as reported previously [24,30].

A window from 0 to 12 $Å^{-1}$ with a cosine edge function was applied to the XAFS data. The Fourier transform had a window applied from 0.5 to 4.5 Å. This window filtered the majority of the atomic XAFS (between 0 and ~1.5 Å).

2.3.1. Determinacy

The number of parameters being fitted, *p*, compared to the number of independent information data points (independent points in the EXAFS plus the number of independent structural parameters), N_i, was calculated to give the degree of determinacy N_i/p. If this ratio is <1, then the model is considered to be underdetermined and a unique fit is not possible. In all cases, the ratio was >1 and, hence, the models were overdetermined. The value of N_i is given by [37]: $N_i = 2(\Delta r)(\Delta k)/\pi + \sum[D(N-2)+1]$; where *D* is the number of dimensions in which the refinement takes place (two for the planar porphyrin and three for the free rotation of the axial groups) and *N* is the number of atoms in the unit. These calculations are combined to give the determinacy values reported in the tables.

2.3.2. Goodness-of-fit (Residual)

The method of determining the goodness of fit was through an *R*-value, where *R* is given by: $R = (\chi^2/\chi^2_{calculated=0})^{1/2}$ where χ^2 is the quantity that was minimized during the refinement and $\chi^2_{calculated=0}$ is the value of χ^2 when the calculated XAFS is uniformly 0 [33]. Residual *R* values of ⩽20% were considered reasonable [35].

2.3.3. Monte-Carlo error analysis

Monte Carlo analyses were conducted to estimate the rms deviations in final parameters arising from the noise in the data. Two consecutive sets of 16 × 16 Monte-Carlo cycles were calculated and the random (statistical) errors due to noise in the data were estimated by Monte-Carlo calculations, and the systematic errors were assigned a conservative value of 0.02 Å.

3. Results

The XANES edge energy of met-IDO2 was at a similar energy to that of met-Mb [24] and met-leghemoglobin (Lb) [38], 7126.5 eV (Fig. 1). However, the shape of the met-IDO2 spectra was similar to that of low-spin met-Lb rather than high-spin met-Mb. The position and structure of the edge spectrum were sensitive indicators of both the local coordination environment and the photodecom-

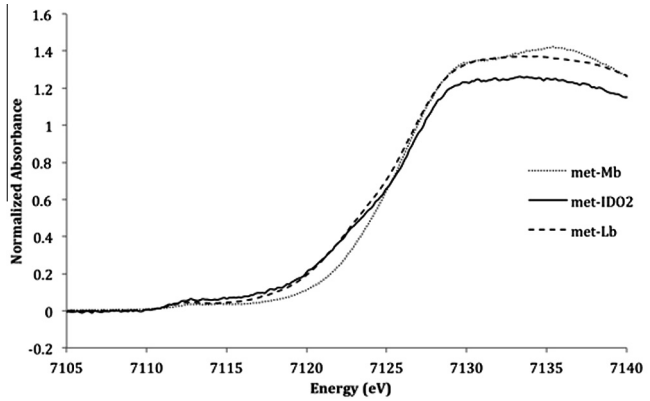

Fig. 1. XANES spectra (10 K) of 40% aqueous glycerol solutions of met-IDO2 and published spectra of met-Mb [24] and met-Lb [38].

position of met-IDO2 during scanning. The edge was monitored during the collection of the data since such proteins are easily reduced to Fe(II) even at 10 K [39]. A shift in the edge energy was evident for subsequent scans, so only the first scan at each position was used.

The XANES and pre-edge regions of the spectra provided significant qualitative information with regard to the symmetry, and spin and oxidation states of the metal. Oyanagi et al. noted that the edge feature at ~7123 eV is observed in low-spin complexes but disappears in high-spin complexes [40]. These changes were evident when the XANES spectra of met-Mb and met-IDO2 were compared (Fig. 1). The met-IDO2 has an edge feature at ~7123 eV, similar to that of the low-spin met-Lb [38], whereas it is absent in the high-spin met-Mb species [24].

A basic five-coordinate model with the Fe–N_p bond length started at 1.99 Å, the Fe–N_e bond length started at 2.0 Å and with free rotation of the imidazole ring gave a poor fit to the EXAFS data (R = 25.3%). However, when a sixth ligand with a nitrogen-bound imidazole ring was included, the residual value dropped to 17.5%, which is a good fit to the data (Table 1, Fig. 2). The structure of the heme moiety of met-IDO2 from the best multiple-scattering (MS) fit to the EXAFS data is shown in Fig. 3 and these results are compared with other models in Table 1. The observed and calculated EXAFS, $\chi(k) \times k^3$, the corresponding Fourier transforms, the residuals, $\Delta[\chi(k) \times k^3]$, and the window functions used in the Fourier filter for the N-bound bis-histidine bound IDO2 for this fit are shown in Fig. 2.

The best fit to the data was obtained using a model with the Fe–N_p bond length started at 1.99 Å, the Fe–N_{HisA} bond length started at 2.0 Å and three-dimensional rotation allowed for both the distal and proximal ligands. The fitted value for Fe–N_p(av) was 2.00 Å, the Fe–N_{HisA} bond length was 2.11 Å and the Fe–N_{HisB} distance was 2.05 Å (R = 18.6%, determinacy 1.12). EXAFS does not distinguish between the distal and proximal histidines and, therefore, it only provided evidence for a bis(His) six coordinate heme iron site with two distinct Fe–N_{His} distances. Experimental details

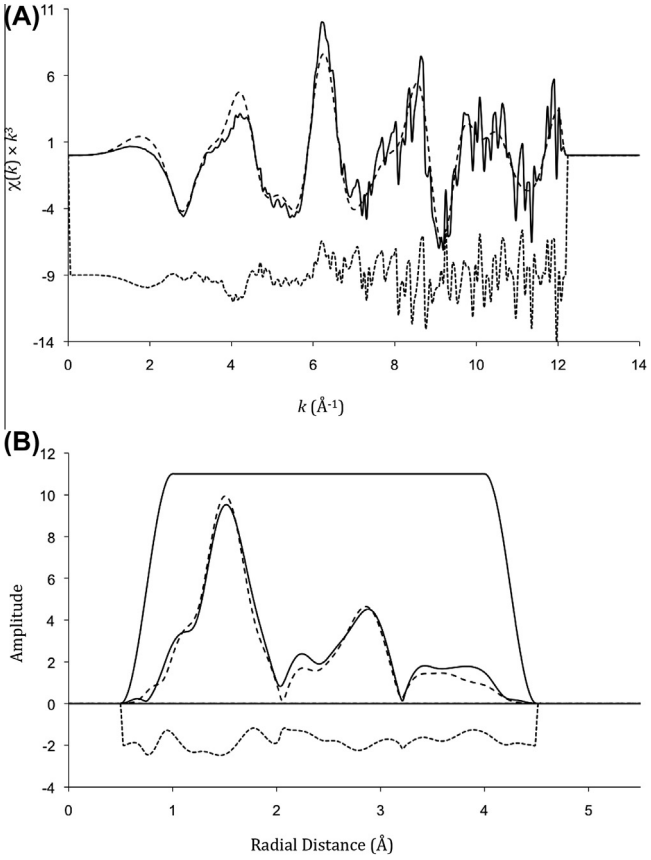

Fig. 2. (A) EXAFS and (B) Fourier transform amplitude of EXAFS of an aqueous/glycerol solution of met-IDO2 at ~10 K.

including paths and importance factors (Table S3) are contained in the Supporting Information.

Other models examined gave worse fits to the data, including a five-coordinate model (25.3%) and six-coordinate models with the sixth ligand being an aqua ligand (24.4%) and *C*-bound histidine, with the *N*-bound histidine planar (20.1%). A model including the entire collected k-range (16 $Å^{-1}$) gave a higher residual (29.9%) due to increased noise levels but showed no change in the fitted parameters, within experimental error, which reinforces the validity of the proposed structure (Table S4). Furthermore, a model with both axial ligands restrained to have the same bond length gave a worse fit to the data (20.6%, Table S4).

4. Discussion

Our previous study of the spectral characteristics of met-IDO2 showed that it is a mixed-spin species at room temperature [16], A similar spin-equilibrium exists for met-IDO1. This has been attributed to a thermal equilibrium between the high-spin aqua (expected to be similar to met-Mb [24]) and low-spin states, with

Table 1
Fe–ligand dimensions as determined by MS EXAFS analyses of met-IDO2.

	Bond lengths (Å)			Mean squared displacement factor ($Å^2$)			Other refinement parameters	
	Fe–N_p	Fe–N_{ax}	Fe–L	Fe–N_p	Fe–N_{zx}	Fe–L	E_o (eV)	R (%)
Five coordinate	1.99	2.12		0.002	0.003		−3.69	25.3
Aqua ligand	2.00	2.15	1.98	0.003	0.004	0.0005	−3.30	24.4
C-bound histidine	2.00	2.08	1.93	0.002	0.001	0.001	−4.37	20.1
N-bound histidine	1.97	2.11	2.05	0.002	0.001	0.001	−4.61	18.6

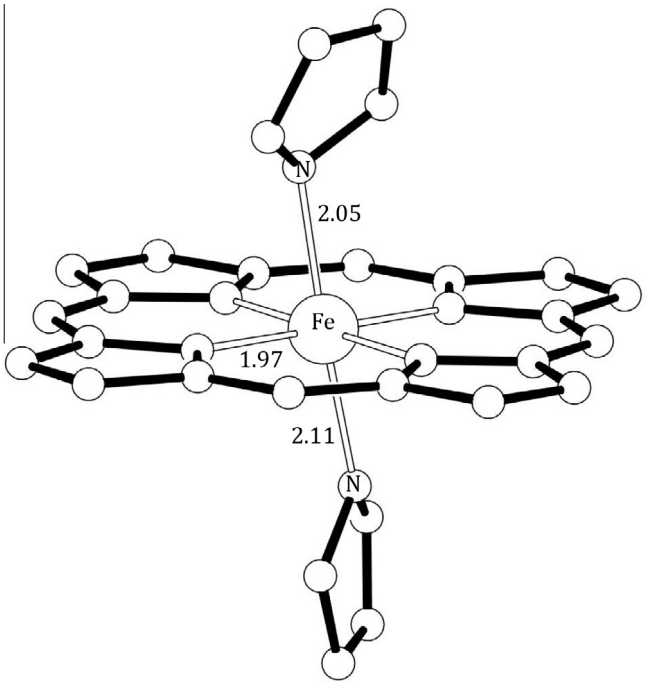

Fig. 3. EXAFS-derived molecular structure of the active site of met-IDO2 at ~10 K.

the low-spin complex predominating as the temperature decreases [41]. At room temperature and neutral pH, the high-spin form of human met-IDO1 dominates with the distal ligand being a weakly bound aqua ligand [42]. However, earlier work had suggested that the sixth ligand of rabbit met-IDO1 was a distal histidine [43]. The crystal structure and the low temperature (10 K) used in this study enabled the determination of the heme structure of the low-spin met-IDO2 species in the equilibrium, as has been observed previously with Lb [44]. Further evidence for the low-spin Fe(III) centre for IDO2 is the bond lengths of the Fe–ligands in comparison to those of met-Mb [24] (Table S2). The bond lengths for Fe–N_p, Fe–N_{ax} are both longer in the met-Mb protein [24] (1.97 Å cf. 2.05 Å and 2.11 Å cf. 2.17 Å, respectively).

The shape of the EXAFS and Fourier transform differs from a typical high-spin Fe(III) heme, such as the aqua adduct in metMb [24] (Figure S2). The electron occupation of the anti-bonding $d_{x^2-y^2}$ and d_{z^2} orbitals in high-spin Fe complexes correlates to longer bond lengths compared to low-spin complexes, where they are unoccupied.

It is evident that such low-spin bis(His) coordination exists in many heme systems and is readily distinguished using EXAFS and XANES analyses from the high-spin met-forms in which the aqua or other oxygen-donor ligands occupy the sixth coordination site [24,35,38,45,46]. In all of these systems the active oxidation state is Fe(II), which binds to O_2 to form Fe(III)-superoxo species. This spectroscopic Fe(III)-superoxo assignment of oxidation states for many of these species in the solution-state has been determined by various techniques, including resonance Raman spectroscopy, XANES and EXAFS [38,46–48]. Like the other heme proteins, IDO1 and IDO2 bind O_2 to the deoxy-protein where, in this case, it is involved in oxidation of substrates and the bis(His) met-form may help to reduce toxicity of the inactive met-form. While there is no evidence, as yet, for a specific binding protein, like there is for α-Hb [46,47], which forces the met-form to adopt a non-toxic bis(His) heme configuration, it is possible that such a protein–protein interaction occurs *in vivo* for both IDO1 and IDO2. This aspect should be explored in the future.

The combined multiple-scattering EXAFS and XANES approach adopted here to determine the structural parameters and nature of axial binding in heme proteins in solution has now been well-established [24,25,30,35,38,47–51], and will be used to follow other aspects of the biochemistry of IDO1 and IDO2 in the future.

5. Conclusions

This is the first three-dimensional structure of the heme environment of the mammalian hemeprotein IDO2. Unlike met-Mb, it has two forms at physiological temperatures, the high-spin form, which is likely to be similar to met-Mb, and a low-spin form, which has shorter bond distances and an *N*-bound bis-histidine structure. It is interesting to speculate on the roles of these two forms since the high-spin met form of many heme proteins is toxic and in some cases, where there is a physiological role, the low-spin bis(His) form is stabilized, as is the case for neuroglobin [45] and the binding of the α-hemoglobin stabilizing protein to α-hemoglobin [46]. There may also be intracellular co-factors for IDO1 and IDO2 that stabilise the low-spin form, while a small equilibrium concentration of the potentially toxic but more reactive high-spin form is required for catalytic activity, and these properties should be investigated in the future.

Acknowledgments

This research was carried out at the Stanford Synchrotron Radiation Lightsource, a Directorate of SLAC National Accelerator Laboratory and an Office of Science User Facility operated for the U.S. Department of Energy Office of Science by Stanford University. The SSRL Structural Molecular Biology Program is supported by the DOE Office of Biological and Environmental Research, and by the National Institutes of Health, National Center for Research Resources, Biomedical Technology Program (P41RR001209). The authors (P.A.L., H.J.B. and N.H.H.) are grateful for funding from the Australian Research Council (ARC Discovery grants). We acknowledge travel funding provided by the International Synchrotron Access Program (ISAP) managed by the Australian Synchrotron. The ISAP was an initiative of the Australian Government being conducted as part of the National Collaborative Research Infrastructure Strategy. We thank Drs Aviva Levina and Farideh Jalilehvand for assistance with gathering of the experimental data.

Appendix A. Supplementary data

Supplementary data associated with this article can be found, in the online version, at http://dx.doi.org/10.1016/j.bbrc.2014.05.054.

References

[1] A.A. Fatokun, N.H. Hunt, H.J. Ball, Indoleamine 2,3-dioxygenase 2 (IDO2) and the kynurenine pathway: characteristics and potential roles in health and disease, Amino Acids 45 (2013) 1319–1329.
[2] Y. Chen, G.J. Guillemin, Kynurenine pathway metabolites in humans: disease and healthy States, Int. J. Tryptophan Res. 2 (2009) 1–19.
[3] S. Adams, N. Braidy, A. Bessede, et al., The kynurenine pathway in brain tumor pathogenesis, Cancer Res. 72 (2012) 5649–5657.
[4] G.W. Beadle, H.K. Mitchell, J.F. Nyc, Kynurenine as an Intermediate in the formation of nicotinic acid from tryptophane by Neurospora, Proc. Natl. Acad. Sci. U.S.A. 33 (1947) 155–158.
[5] O. Hayaishi, S. Rothberg, A.H. Mehler, et al., Studies on oxygenases; enzymatic formation of kynurenine from tryptophan, J. Biol. Chem. 229 (1957) 889–896.
[6] S. Yamamoto, O. Hayaishi, Tryptophan pyrrolase of rabbit intestine. D- and L-tryptophan-cleaving enzyme or enzymes, J. Biol. Chem. 242 (1967) 5260–5266.
[7] H. Ball, A. Sanchez-Perez, S. Weiser, et al., Characterization of an indoleamine 2,3-dioxygenase-like protein found in humans and mice, Gene 396 (2007) 203–213.

[8] R. Metz, J.B. Duhadaway, U. Kamasani, et al., Novel tryptophan catabolic enzyme IDO2 is the preferred biochemical target of the antitumor indoleamine 2,3-dioxygenase inhibitory compound D-1-methyl-tryptophan, Cancer Res. 67 (2007) 7082–7087.
[9] H.J. Yuasa, M. Takubo, A. Takahashi, et al., Evolution of vertebrate indoleamine 2,3-dioxygenases, J. Mol. Evol. 65 (2007) 705–714.
[10] M. Platten, W. Wick, B.J. Van den Eynde, Tryptophan catabolism in cancer: beyond IDO and tryptophan depletion, Cancer Res. 72 (2012) 5435–5440.
[11] C. Uyttenhove, L. Pilotte, I. Theate, et al., Evidence for a tumoral immune resistance mechanism based on tryptophan degradation by indoleamine 2,3-dioxygenase, Nat. Med. 9 (2003) 1269–1274.
[12] C.A. Opitz, U.M. Litzenburger, F. Sahm, et al., An endogenous tumour-promoting ligand of the human aryl hydrocarbon receptor, Nature 478 (2011) 197–203.
[13] A.M. Hansen, C. Driussi, V. Turner, et al., Tissue distribution of indoleamine 2,3-dioxygenase in normal and malaria-infected tissue, Redox Rep. 5 (2000) 112–115.
[14] A.M. Hansen, H.J. Ball, A.J. Mitchell, et al., Increased expression of indoleamine 2,3-dioxygenase in murine malaria infection is predominantly localised to the vascular endothelium, Int. J. Parasitol. 34 (2004) 1309–1319.
[15] H.J. Ball, H.J. Yuasa, C.J. Austin, et al., Indoleamine 2,3-dioxygenase-2; a new enzyme in the kynurenine pathway, Int. J. Biochem. Cell Biol. 41 (2009) 467–471.
[16] C.J. Austin, B.M. Mailu, G.J. Maghzal, et al., Biochemical characteristics and inhibitor selectivity of mouse indoleamine 2,3-dioxygenase-2, Amino Acids 39 (2010) 565–578.
[17] W. Wu, J.A. Nicolazzo, L. Wen, et al., Expression of tryptophan 2,3-dioxygenase and production of kynurenine pathway metabolites in triple transgenic mice and human Alzheimer's disease brain, PLoS One 8 (2013) e59749.
[18] Y. Sun, Indoleamine 2, 3-dioxygenase-a new antioxidant enzyme, Pol. J. Med. Pharm. 21 (1989) 244–250.
[19] M.P. Heyes, K. Saito, J.S. Crowley, et al., Quinolinic acid and Kynurenine pathway metabolism in inflammatory and non-inflammatory neurological disease, Brain 115 (1992) 1249–1273.
[20] T.W. Stone, G.M. Mackay, C.M. Forrest, et al., Tryptophan metabolites and brain disorders, Clin. Chem. Lab. Med. 41 (2003) 852–859.
[21] S. Suzuki, S. Tone, O. Takikawa, et al., Expression of indoleamine 2,3-dioxygenase and tryptophan 2,3-dioxygenase in early concepti, Biochem. J. 355 (2001) 425–429.
[22] M. Sono, T. Taniguchi, Y. Watanabe, et al., Indoleamine 2,3-dioxygenase. Equilibrium studies of the tryptophan binding to the ferric, ferrous, and CO-bound enzymes, J. Biol. Chem. 255 (1980) 1339–1345.
[23] G.J. Maghzal, S.R. Thomas, N.H. Hunt, et al., Cytochrome b5, not superoxide anion radical, is a major reductant of indoleamine 2,3-dioxygenase in human cells, J. Biol. Chem. 283 (2008) 12014–12025.
[24] A.M. Rich, R.S. Armstrong, P.J. Ellis, et al., Determination of iron-ligand bond lengths in horse heart met- and deoxymyoglobin using multiple-scattering XAFS analyses, Inorg. Chem. 37 (1998) 5743–5753.
[25] J.B. Aitken, S.E. Thomas, R. Stocker, et al., Determination of the nature of the heme environment in nitrosyl indoleamine 2,3-dioxygenase using multiple-scattering analyses of X-ray absorption fine structure, Biochemistry 43 (2004) 4892–4898.
[26] G.S. Kachalova, A.N. Popov, H.D. Bartunik, A steric mechanism for inhibition of CO binding to heme proteins, Science 284 (1999) 473–476.
[27] J. Vojtěchovský, K. Chu, J. Berendzen, et al., Crystal structures of myoglobin-ligand complexes at near-atomic resolution, Biophys. J . 77 (1999) 2153–2174.
[28] H. Sugimoto, S. Oda, T. Otsuki, et al., Crystal structure of human indoleamine 2,3-dioxygenase: catalytic mechanism of O_2 incorporation by a heme-containing dioxygenase, Proc. Natl. Acad. Sci. U.S.A. 103 (2006) 2611–2616.
[29] A. Thompson, D. Attwood, E. Gullikson, et al., X-Ray Data Booklet, Lawrence Berkeley National Laboratory, Berkeley, CA, (2001).
[30] A.M. Rich, R.S. Armstrong, P.J. Ellis, et al., Determination of the Fe–ligand bond lengths and Fe–NO bond angles in horse heart ferric and ferrous nitrosylmyoglobin using multiple-scattering XAFS analyses, JACS 120 (1998) 10827–10836.
[31] R. Sundburg, R. Shepherd, H. Taube, Carbon-bound imidazolium ylides as ligands in ruthenium(II) and ruthenium(III) complexes, J. Am. Chem. Soc. 94 (1972) 6558–6559.
[32] J.E. Penner-Hahn, X-ray absorption spectroscopy in coordination chemistry, Coord. Chem. Rev. 192 (1999) 1101–1123.
[33] P.J. Ellis, H.C. Freeman, Xfit – an interactive exafs analysis program, J. Synchrotron Radiat. 2 (1995) 190–195.
[34] J.J. Rehr, R.C. Albers, S.I. Zabinsky, High-order multiple-scattering calculations of X-ray-absorption fine structure, Phys. Rev. Lett. 69 (1992) 3397–3400.
[35] A. Levina, R.S. Armstrong, P.A. Lay, Three-dimensional structure determination using multiple-scattering analysis of XAFS: applications to metalloproteins and coordination chemistry, Coord. Chem. Rev. 249 (2005) 141–160.
[36] J.B. Aitken, E.A. Carter, H. Eastgate, et al., Biomedical applications of X-ray absorption and vibrational spectroscopic microscopies in obtaining structural information from complex systems, Radiat. Phys. Chem. 79 (2010) 176–184.
[37] N. Binsted, R.W. Strange, S.S. Hasnain, Constrained and restrained refinement in EXAFS data analysis with curved wave theory, Biochemistry 31 (1992) 12117–12125.
[38] A. Rich, Determination of Iron-Ligand Bond Lengths and Angles in Hemeproteins Using X-ray Absorption Spectroscopy, School of Chemistry, The University of Sydney, 1997.
[39] G.N. George, I.J. Pickering, M.J. Pushie, et al., X-ray-induced photo-chemistry and X-ray absorption spectroscopy of biological samples, J. Synchrotron Radiat. 19 (2012) 875–886.
[40] H. Oyanagi, T. Iizuka, T. Matsushita, et al., Local-structure of heme-iron studied by high-resolution xanes – thermal spin equilibrium in myoglobin, J. Phys. Soc. Jpn. 56 (1987) 3381–3388.
[41] K. Uchida, T. Shimizu, R. Makino, et al., Magnetic and natural circular dichroism of L-tryptophan 2,3-dioxygenases and indoleamine 2,3-dioxygenase. I. Spectra of ferric and ferrous high spin forms, J. Biol. Chem. 258 (1983) 2519–2525.
[42] A.C. Terentis, S.R. Thomas, O. Takikawa, et al., The heme environment of recombinant human indoleamine 2,3-dioxygenase. Structural properties and substrate-ligand interactions, J. Biol. Chem. 277 (2002) 15788–15794.
[43] M. Sono, J.H. Dawson, Extensive studies of the heme coordination structure of indoleamine 2,3-dioxygenase and of tryptophan binding with magnetic and natural circular dichroism and electron paramagnetic resonance spectroscopy, Biochim. Biophys. Acta 789 (1984) 170–187.
[44] C.A. Appleby, W.E. Blumberg, J. Peisach, et al., Leghemoglobin. An electron paramagnetic resonance and optical spectral study of the free protein and its complexes with nicotinate and acetate, J. Biol. Chem. 251 (1976) 6090–6096.
[45] S. Kakar, F.G. Hoffman, J.F. Storz, et al., Structure and reactivity of hexacoordinate hemoglobins, Biophys. Chem. 152 (2010) 1–14.
[46] L. Feng, D.A. Gell, S. Zhou, et al., Molecular mechanism of AHSP-mediated stabilization of alpha-hemoglobin, Cell 119 (2004) 629–640.
[47] C.F. Dickson, A.M. Rich, W.M. D'Avigdor, et al., Alpha-hemoglobin-stabilizing protein (AHSP) perturbs the proximal heme pocket of oxy-alpha-hemoglobin and weakens the iron-oxygen bond, J. Biol. Chem. 288 (2013) 19986–20001.
[48] S.A. Wilson, E. Green, I.I. Mathews, et al., X-ray absorption spectroscopic investigation of the electronic structure differences in solution and crystalline oxyhemoglobin, Proc. Natl. Acad. Sci. U.S.A. 110 (2013) 16333–16338.
[49] A.M. Rich, P.J. Ellis, L. Tennant, et al., Determination of Fe–ligand bond lengths and the Fe-NO bond angles in soybean ferrous and ferric nitrosylleghemoglobin a using multiple-scattering XAFS analyses, Biochemistry 38 (1999) 16491–16499.
[50] M.C. Cheng, A.M. Rich, R.S. Armstrong, et al., Determination of iron-ligand bond lengths in ferric and ferrous horse heart cytochrome *c* using multiple scattering analyses of XAFS data, Inorg. Chem. 38 (1999) 5703–5708.
[51] C.E. Immoos, F. Sulc, P.J. Farmer, et al., Bonding in HNO-myoglobin as characterized by X-ray absorption and resonance Raman spectroscopies, J. Am. Chem. Soc. 127 (2005) 814–815.